



CHORUS

This is the accepted manuscript made available via CHORUS. The article has been published as:

Confined electronic states and their modulations in graphene nanorings

Jia-Lin Zhu, Xingyuan Wang, and Ning Yang

Phys. Rev. B **86**, 125435 — Published 20 September 2012

DOI: [10.1103/PhysRevB.86.125435](https://doi.org/10.1103/PhysRevB.86.125435)

Confined electronic states and their modulations in graphene nanorings

Jia-Lin Zhu* and Xingyuan Wang

*State Key Laboratory of Low-Dimensional Quantum Physics,
Department of Physics, Tsinghua University, Beijing 100084, China*

Ning Yang

Institute of Applied Physics and Computational Mathematics, P.O. Box 8009(28), 100088 Beijing, China

Confined electronic states in quantum rings formed by spatially modulated finite Dirac gap (FDGQR) in graphene are systematically studied by series-expansion method, and are compared with those in infinite-mass-boundary and one-dimensional quantum rings. The shape-size effect of FDGQR is illustrated to be distinct from that in graphene quantum dots. The Aharonov-Bohm effect in FDGQR is clearly shown by the energy spectrum and the optical-transition probabilities. The FDGQR coupled with the electrostatic-potential induced nanoring is found useful for modulating the Dirac electronic states and the optical-transition probabilities. These results may help to understand and to control the quantum behaviors of confined electronic states in graphene.

PACS numbers: 73.22.Pr, 78.67.Wj, 03.65.Pm

I. INTRODUCTION

Synthesis of graphene¹ has stimulated a renewed interest in the study of the low-dimension quantum systems. Since graphene is true two-dimensional material and exhibits relativistic-like dispersion, it provides a platform to study two-dimensional systems and relativistic quantum mechanics.² Besides, the unique properties of graphene such as the high electron mobility and the valley degeneracy^{1,3,4} make it a promising candidate for future nano-electronics and quantum information devices.

The nanostructures such as nanoribbons,^{2,11} quantum dots,^{2,5,8-14} and quantum rings (QRs)^{2,5-7,11} based on graphene have attracted much attention. It has been illustrated that the confinement of Dirac fermions at a nanometer scale is not trivial due to Klein's paradox,^{15,16} which seriously limits graphene's potential application for building electronic devices, because confining carriers are crucial for applications. Some methods have been proposed to overcome this problem. One way to confine Dirac fermions is to utilize an electrostatic gate by using transverse states in the graphene strip¹⁰ or introducing a gap (rest mass) to graphene systems.¹¹ Another way to confine Dirac fermions is using spatially inhomogeneous magnetic fields.¹² In addition, graphene can be mechanically cut into confinement geometries for electrons.^{13,14}

Recently, the confinement of Dirac fermions by a spatial modulation of the Dirac gap without the application of external electric and magnetic fields is illustrated.⁹ What's more, the QRs based on graphene have become an interesting topic, because the ringlike geometry has special electronic states and allows the investigation of Aharonov-Bohm (AB) effect. In experiment, QRs etched in graphene by lithographic techniques have been investigated and the clear AB conductance oscillations have been observed.¹⁷ In theory, the quantum behaviors of one-dimensional QRs in graphene and finite-width QRs with infinite-mass boundary have been studied in

detail.^{6,7}

In Ref. 6, the analytical expressions for the eigenstates and eigenvalues of carriers confined in one-dimensional QRs have been obtained. Moreover, in Ref. 7, the electronic properties of Aharonov-Bohm rings have been investigated by two different ring systems—a ring with infinite-mass boundary and a hexagonal ring with zigzag edges. Interestingly, a spatially modulated Dirac gap induced by a spatially varying potential of the interface has been reported experimentally in epitaxial graphene.¹⁸ In addition, the local strain and/or chemical methods might also be employed to open up and tune the Dirac gap.^{2,9,19-22} Thus, it is of fundamental interest to investigate the quantum behaviors of the QR formed by a finite Dirac gap (FDGQR) and to reveal the relations to the QRs with infinite-mass boundaries and one-dimensional QRs. More importantly, the incomplete localization of the Dirac fermion in FDGQR permits the coupling between the FDGQR and other quantum systems, then we can study the coupling between the FDGQR and the QR induced by electrostatic potential (EPQR). The distribution of wavefunctions of Dirac fermion and the optical transition probabilities may be tuned by the coupling effect, which are beneficial for applications of graphene. Therefore, in this paper we will explore the size-shape effect of FDGQR along with its AB effect under magnetic flux, and investigate how to modulate the electronic states by coupling FDGQR with EPQR.

The paper is organized as follows: in Sec. II, we present the model of FDGQR in graphene, and the series-expansion method which is employed to calculate its electronic structures. The numerical results and discussion in Sec. III show the size-shape effect, AB effect in FDGQR and the coupling between FDGQR and EPQR, which is followed by a conclusion in Sec. IV.

II. MODEL AND METHOD

The low-energy Dirac fermions in graphene are described by Dirac-Weyl Hamiltonian.²³ Then a QR induced by the modulation of a finite Dirac gap in infinite graphene under electrostatic and magnetic fields is modeled by the Hamiltonian

$$\hat{H}^T = v_F \vec{\sigma} \cdot (\vec{P} + e\vec{A}) + V\mathcal{I} + \tau M\sigma_z, \quad (1)$$

where $v_F \approx 10^6$ m/s is the Fermi velocity, $\vec{P} = -i\hbar(\partial_x, \partial_y)$ is the momentum operator, \vec{A} is the vector potential that generates the magnetic field $\vec{B} = \nabla \times \vec{A}$, V is the electrostatic potential, $\vec{\sigma} = (\sigma_x, \sigma_y)$, σ_z are the 2×2 Pauli operators acting on the two carbon sublattices, \mathcal{I} is the 2×2 unit matrix, M is the Dirac gap, and $\tau = 1$ (-1) labels the K (K') valley.

The FDGQR can be spatially divided into three regions including I ($0 < r \leq R_M - \frac{W_M}{2}$), II ($R_M - \frac{W_M}{2} < r < R_M + \frac{W_M}{2}$), and III ($r \geq R_M + \frac{W_M}{2}$), where W_M and R_M are the width and radius of the FDGQR, respectively. In order to clearly illustrate the quantum behaviors of the FDGQR, we first adopt a discontinuous Dirac gap distribution, expressed as

$$M_S = \begin{cases} M_0 & \text{for regions I and III} \\ 0 & \text{for region II} \end{cases}, \quad (2)$$

where M_0 defines the depth of the QR.

Although the exact form of a spatially modulated gap still needs being investigated experimentally, we also choose a Gaussian profile in this work to simulate a continuously varying gap.

$$M_C = \begin{cases} M_0 & \text{for regions I and III} \\ C[e^{\lambda_0(r-R_M)^2} - 1] & \text{for region II} \end{cases}, \quad (3)$$

where the parameter λ_0 can affect the shape of the QR, and C is chosen so that the M_C is continuous at the interfaces of three regions.

In addition to the spatial modulated gap, a gate electrodes can be suspended above the graphene sheet to spatially modulate the electrostatic potential V .^{24,25} The QRs formed by discontinuous electrostatic potential V can be expressed as

$$V_S = \begin{cases} V_0 & \text{for regions I and III} \\ 0 & \text{for region II} \end{cases}, \quad (4)$$

A slowly varying electrostatic potential V is also chosen as a Gaussian profile.

$$V_C = \begin{cases} V_0 & \text{for regions I and III} \\ C[e^{\lambda_0(r-R_V)^2} - 1] & \text{for region II} \end{cases}, \quad (5)$$

where the meaning of the three regions are similar with those of the FDGQR and the C is chosen so that the V is continuous at the interfaces of three regions. W_V and R_V are the width and radius of the EPQR, respectively.

In the calculations, the cylindrical Dirac gap and electrostatic potential with any kind of radial distributions can be expanded into power series or be approximated by a number of square barriers with different heights. The applied magnetic field $\vec{B} = B\vec{z}$ is perpendicular to the graphene sheet. Under polar coordinates, we adopt the gauge $\vec{A} = (\frac{1}{2}Br + \frac{D}{r})\vec{e}_\theta$, where $D = 0$ for homogeneous magnetic field and $D \neq 0$ for inhomogeneous magnetic field, determined by the continuity of \vec{A} .

For the K valley, the two-component wave function is $\psi^{+1} = (\varphi e^{i\theta}, i\chi e^{i(l+1)\theta})^T$, where φ and χ are the radial parts of the upper and lower components that are used to describe the electronic states in two carbon sublattices of graphene, respectively, i is the imaginary unit, and l is the orbital angular momentum. For convenience, we set the scales of length and energy as $\nu_0 = \sqrt{\hbar}/eB_0$, $E_0 = \hbar v_F/\nu_0$, respectively, and $B_0 = 1$ T. We make the variable substitutions $M/E_0 \rightarrow M$, $D/\nu_0^2 \rightarrow D$, $V/E_0 \rightarrow V$, $B/B_0 \rightarrow B$, and $r/\nu_0 \rightarrow r$. Then from the Hamiltonian in Eq. (1) we can get the equations for the radial functions expressed as

$$\begin{cases} [\frac{d}{dr} + \frac{l+D+1}{r} + \frac{B}{2}r] \chi = (E - V - M)\varphi \\ -[\frac{d}{dr} - \frac{l+D}{r} - \frac{B}{2}r] \varphi = (E - V + M)\chi \end{cases}. \quad (6)$$

To get the eigenenergies and eigenfunctions, we decouple the Eq. (6) and derive two second-order differential equations for the radial functions of upper and lower components. The φ component satisfies

$$-\frac{d^2}{dr^2}\varphi - \frac{1}{r}\frac{d}{dr}\varphi + [-(E - V)^2 + M^2 + (l + 1 + D)B + \frac{(l + D)^2}{r^2} + \frac{B^2}{4}r^2]\varphi = 0. \quad (7)$$

The exact solution of such a differential equation can be obtained from the series expansions around regular singular, ordinary, and irregular singular points, respectively.²⁶

For Eq. (7), the series expansion of the solution in the regular region ($0 \leq r < R_0$) is

$$\varphi = r^{\rho_l} \sum_{n=0}^{\infty} a_n r^n, \quad \rho_l = \sqrt{(l + D)^2}. \quad (8)$$

where the $a_0 \neq 0$. The series expansion of the solution in the irregular region ($R_\infty < r < \infty$) is (see the appendix)

$$\varphi = e^{Q(r)} r^m \sum_{k=0}^{\infty} c_k r^{-k} \quad (9)$$

where

$$Q(r) = \begin{cases} -\frac{|B|r^2}{4} & \text{for } B \neq 0 \\ -\sqrt{M^2 - (E - V)^2}r & \text{for } B = 0 \end{cases}, \quad (10)$$

$$m = \begin{cases} [(E - V)^2 - M^2 + f(B)]/|B| & \text{for } B \neq 0 \\ -1/2 & \text{for } B = 0 \end{cases}, \quad (11)$$

with $f(B) = -|B| - (l+1+D)B$. R_0 and R_∞ are chosen to ensure the proper behaviors of φ in the regular and irregular regions. In the ordinary point region ($R_0 \leq r \leq R_\infty$), we divide it into k small sections $[r_i, r_{i+1}]$, where i is from 0 to $k-1$. The solution in each section is expanded around the center $r_i^c = (r_i + r_{i+1})/2$ as

$$\varphi = C_i \sum_{n=0}^{\infty} c_n (r - r_i^c)^n + D_i \sum_{n=0}^{\infty} d_n (r - r_i^c)^n, \quad (12)$$

where $c_0 = d_1 = 1$, $c_1 = d_0 = 0$. The other values of a_n , b_n , c_n , and d_n ($n > 0$) are determined by recurrence relations.

Using the normalized condition of ψ^{+1} and the matching conditions that φ and χ are continuous at the interface, we obtain the eigenenergies and corresponding a_0 , b_0 , C_i , and D_i , i.e., φ . The corresponding χ can be derived from Eq. (6) as follows

$$\chi = -\frac{1}{E - V + M} \frac{d}{dr} \varphi + \frac{1}{E - V + M} \left(\frac{l+D}{r} + \frac{B}{2} r \right) \varphi. \quad (13)$$

The eigenstates of the K' valley can also be obtained in the same way. For each l , we label the eigenstates of Eq. (7) as (l, n) where $n = 0, 1, 2, \dots$ in the order of the increasing and decreasing eigenenergies for positive and negative eigenenergies, respectively.

III. RESULTS AND DISCUSSION

It is known that the electromagnetic fields do not couple the two valleys K and K' , provided that the fields vary smoothly on the scales of the lattice constant.²⁷ Thus, for the magnetic barrier,¹² homogeneous magnetic field, and the slowly varying electric field, we can solve the Dirac equation in each valley separately in the absence of the inter-valley scattering. Besides, the single-valley condition exists in topological insulators^{28,29} and the fresh presented graphynes³⁰. Therefore, in the following discussion, we consider a valley-polarized situation (K valley) for brevity.

A. Electronic states modulated by Dirac gap

In this section, we investigate the shape-size effect of FDGQR without applying the electrostatic and magnetic fields, i.e., $V = 0$ and $B = 0$. For FDGQR modeled by Eq. (2), Fig. 1(a) shows the Dirac gap M_0 dependence of the energy levels, for $R_M = 50$ nm and $W_M = 20$ nm, with $-3 \leq l \leq 3$ and $0 \leq n \leq 1$. Meanwhile, in Tab. I, we give the energy levels when $M_0=80, 180$ meV and the symbols of the quantum numbers. It shows that, even without applying external electric and magnetic fields, both the electrons and holes can be confined. This can be clearly shown by solution of the series-expansion method at the irregular singular point ($r \rightarrow \infty$). It is well known

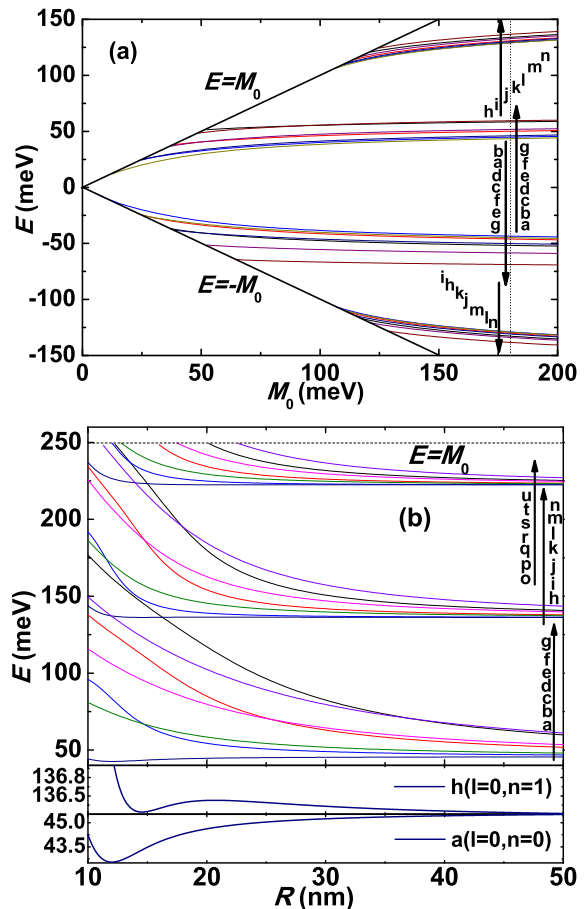


FIG. 1: (Color online) The energy levels of the FDGQR modeled by Eq. (2) for the case of $V = 0$, and $B = 0$ as functions of the (a) M_0 and (b) R_M with $-3 \leq l \leq 3$ and $0 \leq n \leq 1$. The parameters for the rings are (a) $R_M = 50$ nm, $W_M = 20$ nm, and (b) $M_0 = 250$ meV, $W_M = 20$ nm. The symbols a, b, c...representing the quantum numbers (l, n) shown in Tabs. I and II label the energy ordering at (a) $M = 180$ meV and (b) $R_M = 50$ nm.

that, in order to form a confined state, the wavefunction must tend to be zero when $r \rightarrow \infty$, i.e., we should first ensure $M^2 - (E - V)^2 > 0$ for $B = 0$ [See Eq. (9)]. It can also be found from the Eq. (9) that confined states are formed and the number is infinite for $B \neq 0$ as the wavefunction always has a decayed tail when $r \rightarrow \infty$. These conclusions are on the basis of the constant forms of the E , B , and M . It is worthwhile to emphasize that series-expansion method can also be applied to other systems to obtain the criterions for forming confined states by analyzing the confined-deconfined character of the wavefunction at the irregular singular point ($r \rightarrow \infty$).

Fig. 1(a) shows that the confined states gradually emerge from the top or bottom edges ($E = \pm M_0$) of the FDGQR and the absolute value of the energies increases with the increase of the M_0 because the confinement increases. The Dirac fermion with large $|l|$ and n tries to run away from the center of the FDGQR, and

TABLE I: Energy levels of FDGQR in Fig. 1(a) at $M_0 = 80, 180$ and 500 meV. For comparison, the energy levels with infinite-mass boundary are also shown. For convenience, a, b, c, d... are adopted to label the levels. The E^+ and E^- represent the positive and negative energy levels, respectively.

| (l, n) | $E^+(E^-)$ (meV) | | | |
|------------------|---------------------------------|----------------------------------|---------------------------------|--------------------------------|
| | $M_0 = \infty$ | $M_0 = 500$ | $M_0 = 180$ | $M_0 = 80$ |
| a:(0,0) | a(b)51.5801 (-51.5801) | a(b) 48.3722 (-48.3722) | a(b)43.4796 (-43.4796) | a(b)35.9634(-35.9634) |
| b:(-1,0) | b(a)52.6720 (-52.6720) | b(a) 49.5458 (-49.5458) | b(a)44.8294 (-44.8294) | b(a)37.8067(-37.8067) |
| c:(1,0) | c(d)53.8088 (-53.8088) | c(d) 50.7356 (-50.7356) | c(d)46.0676 (-46.0676) | c(d)39.0054(-39.0054) |
| d:(-2,0) | d(c)57.0824 (-57.0824) | d(c) 54.2535 (-54.2535) | d(c)50.1096 (-50.1096) | d(c)44.4069(-44.4069) |
| e:(2,0) | e(f)58.8175 (-58.8175) | e(f) 55.9953 (-55.9953) | e(f)51.7424 (-51.7424) | e(f)45.4308(-45.4308) |
| f:(-3,0) | f(e)64.2662 (-64.2662) | f(e) 61.8478 (-61.8478) | f(e)58.4542 (-58.4542) | g(α)53.7533(-53.7533) |
| g:(3,0) | g(α)65.8696 (-65.8696) | g(α)63.3132 (-63.3132) | g(α)59.4738 (-59.4738) | f(e)54.1874(-54.1874) |
| α :(-4,0) | α (g)73.4818 (-73.4818) | α (g)71.4835 (-71.4835) | α (g)68.8165 (-68.8165) | α (g)65.6266(-65.6266) |
| h:(0,1) | h(i)155.1672(-155.1672) | h(i) 145.4601(-145.4601) | h(i)128.8993(-128.8993) | |
| i:(-1,1) | i(h)155.2993(-155.2993) | i(h) 145.6095(-145.6095) | i(h)129.1342(-129.1342) | |
| j:(1,1) | j(k)156.1949(-156.1949) | j(k) 146.5554(-146.5554) | j(k)130.1086(-130.1086) | |
| k:(-2,1) | k(j)156.5929(-156.5929) | k(j) 147.0060(-147.0060) | k(j)130.8152(-130.8152) | |
| l:(2,1) | l(m)158.3567(-158.3567) | l(m) 148.8638(-148.8638) | l(m)132.7113(-132.7113) | |
| m:(-3,1) | m(l)159.0260(-159.0260) | m(l) 149.6231(-149.6231) | m(l)133.8976(-133.8976) | |
| n:(3,1) | n(β)161.6052(-161.6052) | n(β) 152.3276(-152.3276) | n(β)136.6158(-136.6158) | |
| β :(-4,1) | β (n)162.5554(-162.5554) | β (n) 153.4095(-153.4095) | β (n)138.2990(-138.2990) | |

TABLE II: Energy levels of FDGQR in Fig. 1(b) at $R = 10, 15, 26,$ and 50 nm. For convenience, a, b, c, d... are adopted to label the level ordering.

| (l, n) | E (meV) | | | |
|-----------------|-------------|-------------|-------------|-------------|
| | $R = 50$ nm | $R = 26$ nm | $R = 15$ nm | $R = 10$ nm |
| a:(0,0) | a)45.5101 | a)45.0906 | a)43.4713 | a)44.2451 |
| b:(-1,0) | b)46.7779 | b)50.2535 | b)65.4888 | c)80.9414 |
| c:(1,0) | c)48.0013 | c)53.6970 | c)66.2423 | b)95.9937 |
| d:(-2,0) | d)51.8000 | d)68.8219 | e)94.0114 | e)115.7722 |
| e:(2,0) | e)53.4982 | e)69.0769 | d)109.4355 | d)137.9047 |
| f:(-3,0) | f)59.8129 | g)86.8899 | g)121.5416 | h)143.8978 |
| g:(3,0) | g)61.0570 | f)93.0540 | h)136.2453 | g)149.6042 |
| h:(0,1) | h)136.2131 | h)136.3787 | f)143.3162 | f)176.8420 |
| i:(-1,1) | i)136.3971 | i)137.4010 | i)146.3397 | j)186.3949 |
| j:(1,1) | j)137.3721 | j)141.1689 | j)155.9365 | i)191.8919 |
| k:(-2,1) | k)137.9274 | k)144.4248 | k)183.9422 | l)225.6712 |
| l:(2,1) | l)139.8346 | l)150.9758 | l)185.0007 | k)234.4541 |
| m:(-3,1) | m)140.7716 | m)157.1322 | n)215.5440 | o)237.2452 |
| n:(3,1) | n)143.5289 | n)164.6795 | o)223.1834 | |
| α :(0,2) | o)222.4405 | o)222.4925 | m)223.2250 | |
| p:(-1,2) | p)222.5617 | p)223.3624 | p)231.1708 | |
| q:(1,2) | q)223.1647 | q)225.8110 | q)239.2700 | |
| r:(-2,2) | r)223.5255 | r)227.9264 | | |
| s:(2,2) | s)224.7223 | s)232.5780 | | |
| t:(-3,2) | t)225.3168 | t)235.8401 | | |
| u:(3,2) | u)227.0885 | u)242.1725 | | |

thus, the corresponding states will first disappear with the decrease of the M_0 [as shown in Fig. 1(a)]. Therefore, the density of states in a FDGQR can be tuned low enough by the gap [even only one confined state exist in the FDGQR].

Interestingly, it seems that the $E(l, n) = \pm E_0$ should be established based on the Eq. (7) when $V = 0$. However, it is broken by the inhomogeneous Dirac gap confinement because the confined states with $\pm E_0$, which

satisfy the Eq. (7) and the second-order differential equation of the other component χ , cannot satisfy the Eq. (13) simultaneously. Even in this case, the particle-hole symmetry remains as $E(l, n) = -E(-l - 1, n)$ [See Tab. I]. This can be clearly illustrated by the Eq. (6). If we substitute $l \rightarrow -l - 1$, $E \rightarrow -E$, and $\varphi \leftrightarrow \chi$ into Eq. (6), the Eq. (6) is formally invariant under this transformation. Besides, the $E(j, n) \neq E(-j, n)$ [see Tab. I], where $j = l + 1/2$, since the Dirac gap confinement breaks the effective time-reversal symmetry in a single valley.⁷

Then we briefly discuss the relevance and differences between the FDGQR and QR with infinite-mass boundary. Using the infinite mass boundary condition⁷ $\frac{\partial \psi}{\partial x} = 1(-1)$ at $r = R_M + \frac{W_M}{2}$ ($r = R_M - \frac{W_M}{2}$), we obtain the energy levels of the QRs with infinite-mass boundary. With $R_M = 200$ nm and $W = 20$ nm, we get $E \cdot W_M = 1.5706$ and 1.5749 for states (0,0) and (1,0), respectively, which are consist well with the results in Ref. 7. Then, we calculated the energy levels of QRs with infinite-mass boundary for $R_M = 50$ nm and $W = 20$ nm to compare with the energy levels of FDGQR [See Tab. I]. As shown by the Tab. I, the number of the energy levels of FDGQR is finite and the energy levels of FDGQR are lower than the corresponding energy levels of the QR with infinite-mass boundaries. In addition, the energy level order of FDGQR is different from that of the QR with infinite-mass boundaries when M_0 is small. With the increase of the M_0 , the energy levels of FDGQR gradually approach to that of QR with infinite-mass boundaries. Besides, for large M_0 , the energy level ordering of the low-lying energy levels become the same as that of the QR with infinite-mass boundaries. Therefore, the QR with infinite-mass boundaries is the limitation of the FDGQR with increasing M_0 .

Now, we move on to the size effect of the FDGQR. Fig. 1(b) presents the energy levels as a function of the R_M ,

for $M_0 = 250$ meV and $W_M = 20$ nm, with $-3 \leq l \leq 3$ and $0 \leq n \leq 2$. Meanwhile, in Tab. 2, we give the symbols of the quantum numbers and the energy levels when $R_M = 10, 15, 26, 50$ nm. With $R_M = 10$ nm and $W_M = 20$ nm, it is in fact that the Dirac gap forms a quantum dot. With the increase of the R_M , the system transforms from the quantum dot to the quantum ring and the energy levels show the corresponding transitions. For $R_M \rightarrow \infty$ the energy levels of FDGQR tend to those of a straight two-dimensional wire. It can be found from Eq. (7) that the centrifugal term $[(l+D)^2/r^2]$ of the effective Hamiltonian decreases with the increase of the R_M , which is a factor for the decrease of the absolute values of the energy levels with the increase of the R_M as shown by the energy levels with $l \neq 0$ in Fig. 1(b). Thus, we can decrease the number of confined states in FDGQR by decreasing the R_M . As shown by Fig. 1(b), the confined states with large $|l|$ and n gradually disappear at the top edges of the FDGQR with the decrease of the R_M , because the Dirac fermion with large $|l|$ has large centrifugal force and tends to run away from the center of the FDGQR.

The confinement induced by the outer Dirac gap decreases and the area of region II increases with the increase of the R_M . Both of them lead to the decrease of the absolute values of the energy levels. However, the absolute values of some energy levels with $l = 0$ increase with the increase of the R_M in some range [see the Tab. II and Fig. 1(b)]. This abnormal phenomenon results from the confinement of the inner Dirac gap confinement that tends to push the Dirac fermion out of the region I. The Eq. (8) shows that the upper component of the wave function with $l = 0$ is nonzero at $r = 0$. It feels more compression from the inner Dirac gap. Thus, the absolute values of some energy levels with $l = 0$ increase with the increase of the R_M in some range when the inner Dirac gap confinement dominates the energy levels.

The other effect of the inner confinement of the FDGQR is the variation of the energy level ordering with the increase of the R_M [see Fig. 1(b) and Tab. II]. For example, the energy level orders show angular momentum transition [$f(-3, 0) \leftrightarrow g(3, 0)$] and quantum number n transition [$f(-3, 0) \leftrightarrow h(0, 1)$ and $m(-3, 1) \leftrightarrow o(0, 2)$] at $R_M = 50$ nm \leftrightarrow $R_M = 26$ nm and $R_M = 26$ nm \leftrightarrow $R_M = 15$ nm, respectively. The change of the energy level is determined by the inner Dirac gap confinement, outer Dirac gap confinement, and the distribution of the state. The combined effect of inner and outer Dirac gap confinement leads to the change of the energy level ordering. It is worthwhile to point out that the anomalous increase of the absolute values of energy levels mentioned above and the variation of the energy level ordering with the increase of the R_M are absent in the Dirac gap quantum dot because it only has the outer Dirac gap confinement.

What is discussed above clearly shows that in FDGQR, both the energy levels and the density of confined states can be tuned by the depth of Dirac gap and the radius of the quantum ring. The ordering of the energy levels and

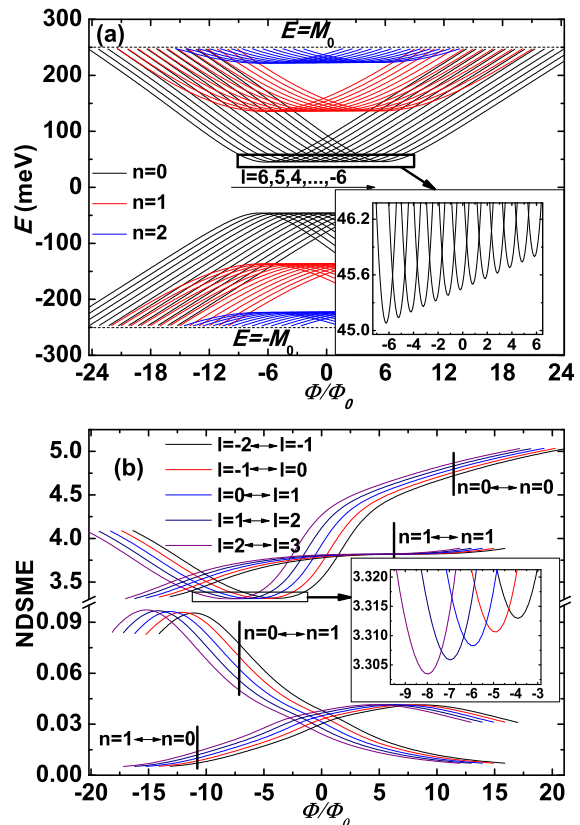


FIG. 2: (Color online) (a) The magnetic flux Φ dependence of the energy levels of a FDGQR described by Eq. (2) with $-6 \leq l \leq 6$ and $0 \leq n \leq 2$. The parameters are $R_M = 50$ nm, $W_M = 20$ nm, $M_0 = 250$ meV, and $V = 0$. (b) The corresponding Φ dependence of the NDSME between the positive energy levels (l, n) and (l', n') in (a).

angular momentum transitions may be changed as well. These characteristics are helpful in the manipulation of quantum behaviors in graphene nanorings.

B. Electronic states modulated by magnetic field

In order to investigate the AB effect in FDGQR described by Eq. (2), we suppose that the magnetic field only threads through region I and is zero in regions II and III, which creates a magnetic flux $\Phi = \pi(R_M - \frac{W_M}{2})^2 B$ through region I. Fig. 2(a) shows the magnetic flux Φ dependence of the energy levels, for $R_M = 50$ nm, $W_M = 20$ nm, $M_0 = 250$ meV, and $V = 0$, with $-6 \leq l \leq 6$ and $0 \leq n \leq 2$. In order to clearly show the physical picture, we present the energy levels in a large variation range of Φ . In fact, we need to focus only on the range of $-6 < \frac{\Phi}{\Phi_0} < 6$ [about -4.94 T $< B < 4.94$ T] which can be easily achieved in experiments. As the Dirac fermion is mostly localized in region II, it hardly feels the magnetic field except being affected by the magnetic vector potential. From Eq. (6), we can find that the

Dirac fermion localized in region II has an effective orbital angular momentum

$$l^* = l + \frac{\Phi}{\Phi_0}, \quad (14)$$

where $\Phi_0 = \frac{h}{e}$ is the quantum of magnetic flux [with a magnetic flux Φ through region I and $B = 0$ in region II and III, $D = \frac{\Phi}{\Phi_0}$ in regions II and III]. Therefore, the energy ordering based on the angular momentum can be changed by changing the effective orbital angular momentum, which shows the angular momentum oscillates with the magnetic flux [See Fig. 2(a)]. Every energy level will show a minimum at a certain Φ . With the increase of the Φ , the minima of the energies for different l appear in the order of decreasing l . These characteristics of energy spectrum, i.e. the AB effect, are similar with those of QR with infinite mass boundary⁷ and one-dimensional QR⁶, which show that the space of Φ for the nearest-neighbor minima is Φ_0 and the minima of the energy levels of different l are the same. However, the Dirac fermion in FDGQR is not completely localized in region II due to the finite Dirac gap. Therefore, the space of Φ for two neighbor minima of the energy levels of FDGQR is not exactly Φ_0 . And the minima of the energy levels of different l are not the same absolutely, but increase with the decrease of the l [see the inset of Fig. 2(a)]. Besides, any confined state exists only in a certain region of Φ and they become deconfined when the Φ is outside this region [see Fig. 2(a)].

From above discussions, it can be seen that the main characteristics of AB oscillation of the energy levels in FDGQR are similar with one-dimensional QRs where the radial motion of carriers is frozen out. However, the finite width and finite height of the ring's confinement bring new characteristics to the energy spectrum. The radial motion and the AB effects may be observed in optical experiments, so we now turn to discuss the modulation of the magneto-optical properties of FDGQR. In the electric dipole approximation, the optical transitions stimulated by a left (right) circular polarized light which is perpendicular to the graphene sheet are related to the squared transition matrix element $|\langle \psi_f | r e^{-i\theta} | \psi_i \rangle|^2$. Under the scales in this paper, the non-dimensionalized squared matrix element (NDSME) can be calculated as $|2\pi \int_0^\infty dr r^2 (\varphi_i \varphi_f + \chi_i \chi_f) \delta_{l_i - l_f \mp 1}|^2$. Considering the conservation of angular momentum, the angular momentum provided by the left (right) circular polarized light demands that the selection rule should satisfy $l_i \mp l_f = 1$, where $-(+)$ corresponds to the left (right) circular polarized light. Fig. 2(b) shows the Φ dependence of the NDSME between the positive energy levels of $0 \leq n \leq 1$ and $-2 \leq l \leq 2$ in Fig. 2(a). The NDSME can be remarkably tuned by the Φ [see Fig. 2(b)], which reflects the characteristics of the energy spectrum. At certain Φ , the NDSMEs show extremums. The minima appear in the order of decreasing l_i with the increase of Φ , similar to the energy spectrum, which is a reflection of AB effect. Besides, for the parameters used in this paper, the

NDSME of the transition between the confined states with the same n is approximately two order larger than that of the transition between the confined states with different n .

It is worthwhile to point out that we also calculated the spectrum when the homogeneous magnetic field is perpendicularly applied in the whole area. In this case the confined states still exist when $|E| > M_0$ because of the confinement of the magnetic field. Thus, the number of confined states is infinite. For the homogeneous magnetic field, the Dirac fermion can feel the magnetic field in addition to Φ . However, the AB effect reflected by the change of the angular momentum is still obvious. In addition, the AB effect in small-size FDGQR is more obvious. This is because the spaces among energy levels are generally large for small-size FDGQR [see Fig. 1(b)] and then the energy levels change in a large range with the change of Φ and form a clear AB oscillation.

C. Coupling between EPQR and FDGQR

In this section, we explore a coupled system formed by EPQR and FDGQR. At first, Both of the two kinds of QRs are chosen as the discontinuous profiles described by Eq. (2) and Eq. (4), respectively. With $B = 0$, we choose the parameters $R_M = 25$ nm, $W_M = 10$ nm, and $M_0 = 250$ meV for FDGQR and $W_V = 10$ nm, and $V_0 = 250$ meV for the EPQR. The energy levels as the function of R_V are presented in Fig. 3(a). It can be seen from the Eq. (9) that, for $B = 0$ and $V = M$, the energy levels of the confined states should satisfy $0 < E < V + M$, as the same as the results shown in Fig. 3(a).

When the $|R_V - R_M|$ is large, the classically forbidden barrier between the EPQR and the FDGQR is large. Thus, the coupling between EPQR and FDGQR is weak and the electron is mostly confined in either EPQR or FDGQR. Here the EPQR and FDGQR refer to the spatial divisions as shown by Fig. 3(b)-Fig. 3(g). In this case, the energy levels in Fig. 3(a) with $n = 2, 4$ and $n = 0, 1, 3, 5$ are similar with the energy levels of the single EPQR with $M = M_0$ and the FDGQR, respectively. These can be clearly shown by the distributions of the wavefunctions. It can be seen that the states (1,3) [See Fig. 3(b) and Fig. 3(d)] and (1,2) [See Fig. 3(e) and Fig. 3(g)] mostly localize in the FDGQR and EPQR, respectively. Thus, most of the energy levels with $n = 2, 4$ monotonously decrease but some energy levels with $l = 0$ do not monotonously decrease with the increase of the R_V , which is similar to the size effect of the FDGQR [see the discussion in section A]. In contrast, the energy levels with $n = 0, 1, 3$, and 5 are almost independent of the R_V for large $|R_V - R_M|$. It should be pointed out that though the $|R_V - R_M|$ is large the state (1,3) has some probability in EPQR [see Fig. 3(b)], this is because the energy levels (1,3) and (1,2) are very close at those parameters.

As the $|R_V - R_M|$ decreases, the coupling between

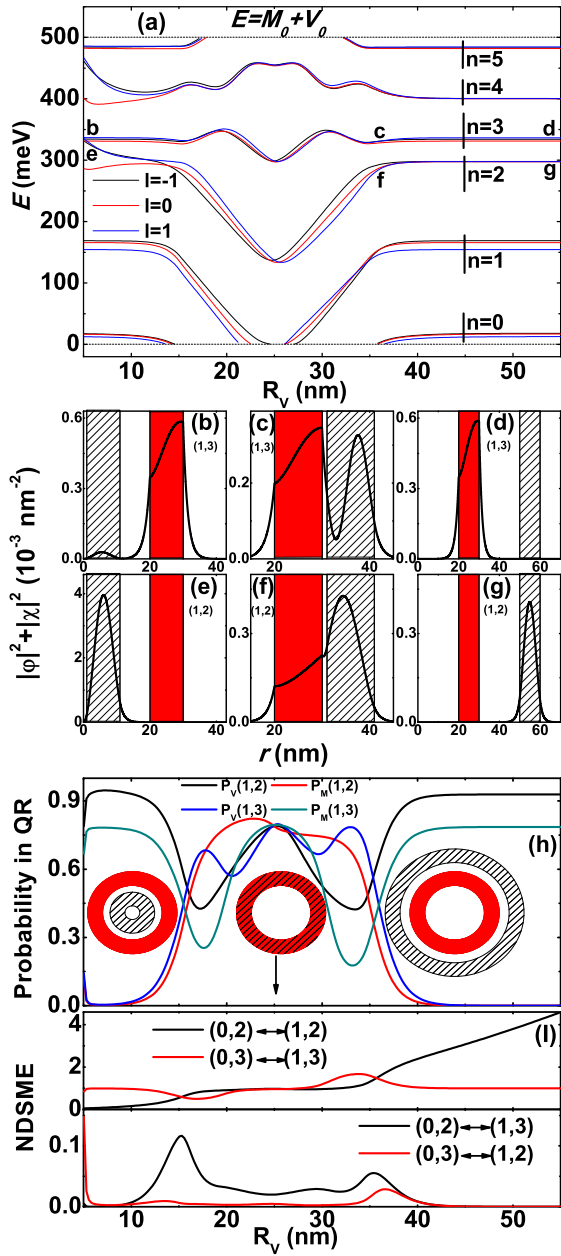


FIG. 3: (Color online) (a) The R_V dependence of the energy levels for coupled FDGQR and EPQR with $-2 \leq l \leq 2$. The coupled FDGQR and EPQR are modeled by Eq. (2) and Eq. (4), respectively. The parameters are $R_M = 25$ nm, $W_M = 10$ nm, $M_0 = 250$ meV, $W_V = 10$ nm, $V_0 = 250$ meV, and $B = 0$. (b)-(g) The radial distribution of the states (1,3) and (1,2) at positions marked by b-g in (a), where the regions filled with black slanted lines and the red color represent the regions II of EPQR and FDGQR, respectively. (h) The probability that the Dirac fermion appears in the regions II of EPQR [$P_V(l, n)$] and FDGQR [$P_M(l, n)$]. (i) The R_V dependence of the NDSME. The insets in (h) are schematic diagrams of the systems, where the ring filled with black slanted lines and the red ring represent the EPQR and FDGQR, respectively.

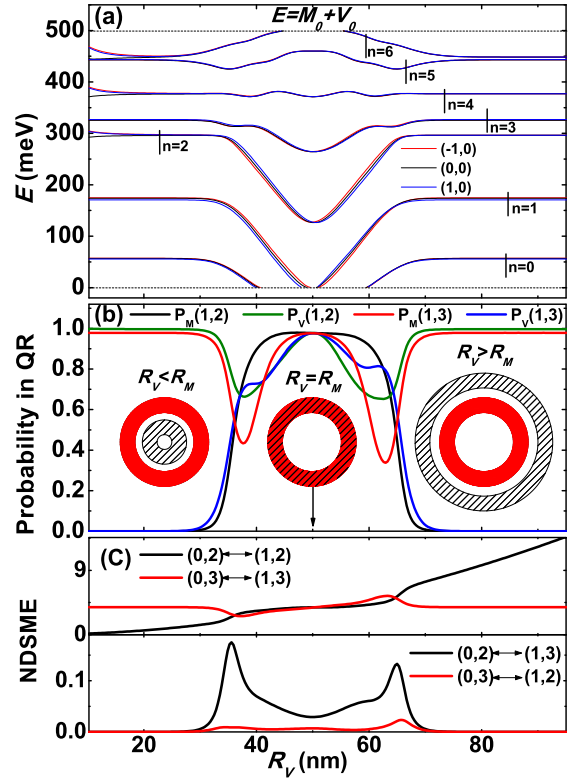


FIG. 4: (Color online) (a) The R_V dependence of the energy levels for coupled FDGQR and EPQR with $-2 \leq l \leq 2$. The coupled FDGQR and EPQR are modeled by Eq. (3) and Eq. (5), respectively. The parameters are $R_M = 50$ nm, $W_M = 20$ nm, $M_0 = 250$ meV, $W_V = 20$ nm, $V_0 = 250$ meV, $\lambda_0 = 1/\nu_0^2$, and $B = 0$. (b) The probability that the Dirac fermion appears in the regions II of EPQR [$P_V(l, n)$] and FDGQR [$P_M(l, n)$]. (c) The R_V dependence of the NDSME. The insets in (b) are schematic diagrams of the systems, where the ring filled with black slanted lines and the red ring represent the EPQR and FDGQR, respectively.

EPQR and FDGQR becomes strong. As shown by Fig. 3(c) and Fig. 3(f), the wavefunctions become extension within the FDGQR and EPQR and the energy levels began to deviate from the spectrums of the single FDGQR or EPQR with $M = M_0$. When the $|R_V - R_M|$ is smaller than 10 nm, the FDGQR overlaps with the EPQR. In this case, the energy levels can be strongly tuned by the R_V and show minima or maxima. In addition, the states with $n = 0, 1, 5$ in Fig. 3(a) become deconfined at some critical points of $|R_V - R_M|$.

In order to clearly show the coupling effect and the modulation of the spatial distribution of the hybridized-state, we plot the probabilities that the Dirac fermion appears in either EPQR or FDGQR (in regions II of either EPQR or FDGQR) as a function of R_V , where $P_V(l, n)$ and $P_M(l, n)$ represent the probability that the Dirac fermion appears in EPQR and FDGQR, respectively [see Fig. 3(h)]. When the $|R_V - R_M|$ is large, the Dirac fermion of state (1,2) [(1,3)] is localized in

the EPQR [FDGQR] and the probability that the Dirac fermion appears in the FDGQR [EPQR] is almost zero [see Fig. 3(h)]. With the decrease of the $|R_V - R_M|$, the probability that the Dirac fermion appears in EPQR [FDGQR] begins to decrease [see Fig. 3(h)] because the coupling becomes strong and the Dirac fermion gradually transfers from the EPQR [FDGQR] to the FDGQR [EPQR]. Besides, the Dirac fermion begins to transfer from the EPQR [FDGQR] to the FDGQR [EPQR] when $R_V \sim 6$ nm, which illustrated that the coupling becomes strong when the energy levels of states (1,2) and (1,3) are very close.

In Fig. 3(I), we shows the R_V dependence of the NDSME. In this paragraph, we discuss the case of $R_V - R_M > 10$ nm to illustrate that the NDSME depends on the spatial distribution of the wavefunctions and to show the modulation of NDSME by tuning the spatial distribution of the wavefunctions. In this case, the electronic states of $n = 3$ are localized almost in the FDGQR, which tend to be unchanged with the increase of $R_V - R_M$. Thus, the NDSME between the electronic states with $n = 3$ is almost constant, weakly affected by R_V . In contrast, the electronic states of $n = 2$ are localized almost in the EPQR for $R_V - R_M > 10$ nm, Therefore, the NDSME between the electronic states with $n = 2$ is strongly tuned by the R_V and monotonously increases with the increase of the R_V because the NDSME $|2\pi \int_0^\infty dr r^2 (\varphi_i \varphi_f + \chi_i \chi_f) \delta_{i-l_f-1}|^2$ is related to r .

To step further, we illustrate that the NDSME is related to the overlap between the wavefunctions of the final and initial states and show the modulation of the NDSME by tuning the overlap of the wavefunctions. As shown by Fig. 3(I), the magnitude of the NDSME between the electronic states with the same n is approximately two order larger than that between the electronic states with different n for the parameters in this paper because the overlap of the wavefunctions with the same n is larger than that with different n . It is well known that the small energy space is advantageous for the stimulated transition. However, though the energy space between the energy levels with $n = 2$ and $n = 3$ in Fig. 3(I) is small for $R_V - R_M > 10$ nm, the NDSME is almost zero and the stimulated transition is forbidden. This is because the electronic states of $n = 2$ and $n = 3$ are localized in EPQR and FDGQR, respectively, and their wavefunctions have little overlap. For $|R_V - R_M| < 10$ nm, the energy space between energy levels of $n = 2$ and $n = 3$ is larger than that of $R_V - R_M > 10$ nm, but the NDSME is larger than that of $R_V - R_M > 10$ nm because of the increasing overlap of the wavefunctions.

One might wonder how the results will change if we have smooth interfaces instead of the step potential. Here we consider a smooth interface of the Gaussian profile as described by Eq. (3) and Eq. (5), respectively. With $B = 0$, we choose the parameters $R_M = 50$ nm, $W_M = 20$ nm, $M_0 = 250$ meV, and $\lambda_0 = 1/\nu_0^2$ for FDGQR and $W_V = 20$ nm, $V_0 = 250$ meV, and $\lambda_0 = 1/\nu_0^2$ for the EPQR. It can be seen in Fig. 4 that the results are qual-

itatively similar with the results of step potential. On the other hand, When the $|R_V - R_M|$ is large, the probability that the Dirac fermion state (1,2) [(1,3)] appears in the FDGQR [EPQR] is almost 1 [see Fig. 4(b)], which is larger than that in Fig. 3(h). This means that the coupling effect of the QRs with large width is more weaker than that of the QRs with small width.

Therefore, the coupling of the EPQR and FDGQR is useful for modulating the quantum states and the optical property in graphene nanorings.

IV. CONCLUSION

In summary, we have explored quantum rings formed by spatially modulated finite Dirac gap (FDGQR) by exactly expanding the wavefunctions around regular, irregular and ordinary points, respectively in the form of series. The criterion of the existence of confined states is given by analyzing the asymptotic behaviors of the series-expansion wavefunctions around the irregular point ($r \rightarrow \infty$). A finite number of confined states can exist in the FDGQR without the application of external fields. The change of the energy level ordering and unusual increase of the absolute values of some low-lying energy levels with the increase of the radius of the FDGQR are illustrated, which are absent in the graphene quantum dots. The energy spectrum and the optical-transition probabilities clearly show the AB effect of the incompletely localized Dirac fermion. The Dirac fermion in the coupled FDGQR and EPQR can be localized almost in the FDGQR or EPQR and the optical-transition probabilities can be tuned. These results may be useful for understanding and controlling the quantum behaviors of confined electronic states in graphene. Besides, the exact series-expansion method provides a way to obtain the state-confinement criterion.

Acknowledgments

Financial supports from NSF China (Grant No. 10974108 and 11174170) and the "973" Programme of China (No. 2011CB921901) are gratefully acknowledged.

Appendix: The derivation of the asymptotic solution for $r \rightarrow \infty$

The Eq. (6) can be rewritten in the general form

$$\left\{ \frac{d^2}{dr^2} + \frac{1}{r} \frac{d}{dr} - \sum_{i=-2}^K w_i r^i \right\} \varphi(r) = 0. \quad (\text{A.1})$$

For $r > R_\infty$, the irregular solution can be written in the form

$$\varphi(r) = e^{Q(r)} r^m \sum_{k=0}^N c_k r^{-k}, \quad (\text{A.2})$$

with

$$Q(r) = \sum_{i=0}^{N_c} q_i r^i, \quad (\text{A.3})$$

where $c_0 \neq 0$. Substituting the Eq. (A.2) into the Eq. (A.1), we can obtain the following form

$$\left[\frac{d^2}{dr^2} + p(r) \frac{d}{dr} + q(r) \right] r^m \sum_{k=0}^N c_k r^{-k} = 0, \quad (\text{A.4})$$

where

$$p(r) = 2 \sum_{i=1}^{N_c} i q_i r^{i-1} + \frac{1}{r}, \quad (\text{A.5})$$

$$q(r) = \sum_{i=2}^{N_c} i(i-1) q_i r^{i-2} + \sum_{i=1}^{N_c} i q_i r^{i-2} + \left(\sum_{i=1}^{N_c} i q_i r^{i-1} \right)^2 - \sum_{i=-2}^K w_i r^i. \quad (\text{A.6})$$

The order of the series $p(r)$ must be larger than the order of the series $q(r)$ in order to ensure that the equation has solutions. The coefficients of the terms of $q(r)$, whose powers are larger than $N_c - 2$ must be zero. Therefore, we get the relations

$$\begin{cases} N_c = K/2 + 1 \\ \sum_{i=j-N_c+2}^{N_c} i(j+2-i) q_i q_{j+2-i} = w_j, \end{cases}, \quad (\text{A.7})$$

where $j = N_c - 1, N_c, \dots, 2(N_c - 1)$. Based on Eq. (A.7), we can obtain

$$\begin{cases} q_{N_c} = -\sqrt{w_K}/N_c \\ q_i = \frac{1}{2iN_c q_{N_c}} \\ \left[w_{i+N_c-2} - \sum_{m=i+1}^{N_c-1} m(i-m+N_c) q_{i-m+N_c} q_m \right] \end{cases}. \quad (\text{A.8})$$

Then, the Eq. (A.3) is available:

$$Q(r) = \begin{cases} -\frac{|B|r^2}{4} & (B \neq 0) \\ -\sqrt{-(E-V)^2 + M^2} r & (B = 0) \end{cases}. \quad (\text{A.9})$$

Substituting the obtained Eq. (A.9) into Eq. (A.4), we can get the m of the Eq. (A.2) as follows

$$m = \begin{cases} [(E-V)^2 - M^2 + f(B)]/|B| & \text{for } B \neq 0 \\ -1/2 & \text{for } B = 0 \end{cases}, \quad (\text{A.10})$$

with $f(B) = -|B| - (l+1+D)B$. Then, we can obtain the recurrence relations for c_k of the Eq. (A.2)

$$c_k = \frac{1}{a_0 k} \left\{ \sum_{i=1}^{\min(k, n_1+1)} [a_i(m-k+i) + b_i] c_{k-i} + c_{k-n_1-1} (m-k+n_1+1)(m-k+n_1) \right\}, \quad (\text{A.11})$$

where the parameters are $n_1 = 1$, $a_0 = -|B|$, $a_1 = 0$, $a_2 = 1$, $b_1 = 0$, and $b_2 = -(l^2 + 2lD + D^2)$ for $B \neq 0$, and $n_1 = 0$, $a_0 = -2\sqrt{-(E-V)^2 + M^2}$, $a_1 = 1$, and $b_1 = -l^2$ for $B = 0$.

* Electronic address: zjl-dmp@tsinghua.edu.cn

¹ K. S. Novoselov, A. K. Geim, S. V. Morozov, D. Jiang, Y. Zhang, S. V. Dubonos, I. V. Grigorieva, and A. A. Firsov, *Science* **306**, 666 (2004).

² A. H. Castro Neto, F. Guinea, N. M. R. Peres, K. S. Novoselov and A. K. Geim, *Rev. Mod. Phys.* **81**, 109 (2009).

³ A. Cresti, N. Nemeč, B. Biel, G. Niebler, F. Triozon, G. Cuniberti, and S. Roche, *Nano Res.* **1**, 361 (2008).

⁴ A. K. Geim, *Science* **324**, 1530 (2009).

⁵ C. A. Downing, D. A. Stone, and M. E. Portnoi, *Phys. Rev. B* **84**, 155437 (2011).

⁶ M. Zarenia, J. M. Pereira, A. Chaves, F. M. Peeters, and G. A. Farias, *Phys. Rev. B* **81**, 045431 (2010).

⁷ P. Recher, B. Trauzettel, A. Rycerz, Ya. M. Blanter, C. W. J. Beenakker, and A. F. Morpurgo, *Phys. Rev. B* **76**, 235404 (2007).

⁸ T. Paananen, R. Egger, and H. Siedentop, *Phys. Rev. B* **83**, 085409 (2011).

⁹ G. Giavaras, and F. Nori, *Phys. Rev. B* **83**, 165427 (2011).

¹⁰ P. G. Silvestrov, and K. B. Efetov, *Phys. Rev. Lett.* **98**, 016802 (2007).

¹¹ P. Recher, B. Trauzettel, *Nanotechnology* **21**, 302001 (2010).

¹² A. De Martino, L. Dell'Anna, and R. Egger, *Phys. Rev. Lett.* **98**, 066802 (2007).

¹³ A. V. Rozhkov, and F. Nori, *Phys. Rev. B* **81**, 155401 (2010).

¹⁴ F. Libisch, S. Rotter, J. Güttinger, C. Stampfer, and J. Burgdörfer, *Phys. Rev. B* **81**, 245411 (2010).

¹⁵ O. Klein, *Z. Phys.* **53**, 157 (1929).

¹⁶ M. I. Katsnelson, K. S. Novoselov, and A. K. Geim, *Nat. Phys.* **2**, 620 (2006).

¹⁷ Saverio Russo, Jeroen B. Oostinga, Dominique Wehenkel,

- Hubert B. Heersche, Samira Shams Sobhani, Lieven M. K. Vandersypen, and Alberto F. Morpurgo, *Phys. Rev. B* **77**, 085413 (2008).
- ¹⁸ L. Vitali, C. Riedl, R. Ohmann, I. Brihuega, U. Starke, and K. Kern, *Surf. Sci.* **602**, 127 (2008).
- ¹⁹ D. S. L. Abergel, V. Apalkov, J. Berashevich, K. Ziegler, and T. Chakraborty, *Adv. Phys.* **59**, 261 (2010).
- ²⁰ A. V. Rozhkov, G. Giavaras, Y. P. Bliokh, V. Freilikher, and F. Nori, *Phys. Reports* **503**, 77 (2011).
- ²¹ G. Giovannetti, P. A. Khomyakov, G. Brocks, P. J. Kelly, and J. van den Brink, *Phys. Rev B* **76**, 073103 (2007).
- ²² R. P. Tiwari and D. Stroud, *Phys. Rev. B* **79**, 205435 (2009).
- ²³ G. W. Semenoff, *Phys. Rev. Lett.* **53**, 2449 (1984).
- ²⁴ J. Velasco, Jr., G. Liu, W. Bao, and C. N. Lau, *New J. Phys.* **11**, 095008 (2009).
- ²⁵ R. V. Gorbachev, A. S. Mayorov, A. K. Savchenko, D. W. Horsell, and F. Guinea, *Nano Lett.* **8**, 1995 (2008).
- ²⁶ J. L. Zhu, *Phys. Rev. B* **39**, 8780 (1989).
- ²⁷ C. W. J. Beenakker, *Rev. Mod. Phys.* **80**, 1337 (2008).
- ²⁸ K. Chang and W. K. Lou, *Phys. Rev. Lett.* **106**, 206802 (2011).
- ²⁹ M. Z. Hasan and C. L. Kane, *Rev. Mod. Phys.* **82**, 3045 (2010).
- ³⁰ D. Malko, C. Neiss, F. Viñes, and A. Görling, *Phys. Rev. Lett.* **108**, 086804 (2012).